The Astrophysical Journal, 963:125 (13pp), 2024 March 10 https://doi.org/10.3847/1538-4357/ad1bcf

Recovering Lost Light: Discovery of Supernova Remnants with Integral Field Spectroscopy

Héctor Martínez-Rodríguez[1], Lluís Galbany[2,3], Carles Badenes[1], Joseph P. Anderson[4,5], Inmaculada Domínguez[6], Hanindyo Kuncarayakti[7], Joseph D. Lyman[8], Sebastián F. Sánchez[9], José M. Vílchez[10], Nathan Smith[11], and Dan Milisavljevic[12,13]

[1] Department of Physics and Astronomy and Pittsburgh Particle Physics, Astrophysics and Cosmology Center (PITT PACC), University of Pittsburgh, 3941 O'Hara Street, Pittsburgh, PA 15260, USA; hector.mr@pitt.edu
[2] Institute of Space Sciences (ICE, CSIC), Campus UAB, Carrer de Can Magrans, s/n, E-08193 Barcelona, Spain
[3] Institut d'Estudis Espacials de Catalunya (IEEC), c. Gran Capità, 2-4, E-08034 Barcelona, Spain
[4] European Southern Observatory, Alonso de Córdova 3107, Vitacura, Casilla 190001, Santiago, Chile
[5] Millennium Institute of Astrophysics MAS, Nuncio Monsenor Sotero Sanz 100, Off. 104, Providencia, Santiago, Chile
[6] Departamento de Física Teórica y del Cosmos, Universidad de Granada, E-18071 Granada, Spain
[7] Tuorla Observatory, Department of Physics and Astronomy, University of Turku, Väisäläntie 20, FI-21500 Piikkiö, Finland
[8] Department of Physics, University of Warwick, Coventry, CV4 7AL, UK
[9] Instituto de Astronomía, Universidad Nacional Autónoma de México, A.P. 70-264, C.P. 04510, México, D.F., Mexico
[10] Instituto de Astrofísica de Andalucía—CSIC, Glorieta de la Astronomía s.n., E-18008 Granada, Spain
[11] Steward Observatory, University of Arizona, 933 N. Cherry Aveue, Tucson, AZ 85721, USA
[12] Department of Physics and Astronomy, Purdue University, West Lafayette, IN 47907, USA
[13] Integrative Data Science Initiative, Purdue University, West Lafayette, IN 47907, USA
Received 2023 September 21; revised 2024 January 4; accepted 2024 January 4; published 2024 March 6

Abstract

We present results from a systematic search for broad ($\geqslant 400\,\mathrm{km\,s^{-1}}$) H$\alpha$ emission in integral field spectroscopy data cubes of ∼1200 nearby galaxies obtained with PMAS and MUSE. We found 19 unique regions that pass our quality cuts, four of which match the locations of previously discovered supernovae (SNe): one Type IIP and three Type IIn, including the well-known SN 2005ip. We suggest that these objects are young Supernova remnants (SNRs), with bright and broad Hα emission powered by the interaction between the SN ejecta and dense circumstellar material. The stellar ages measured at the locations of these SNR candidates are systematically lower by about 0.5 dex than those measured at the locations of core-collapse (CC) SNe, implying that their progenitors might be shorter lived and therefore more massive than a typical CCSN progenitor. The methods laid out in this work open a new window into the study of nearby SNe with integral field spectroscopy.

Unified Astronomy Thesaurus concepts: Supernova remnants (1667); Stellar feedback (1602); Interstellar medium (847); Galaxies (573); Core-collapse supernovae (304)

1. Introduction

Supernovae (SNe) are energetic stellar explosions that mark the endpoints in the lives of certain types of stars. Although they are rare events, occurring once or twice per century in a typical galaxy, SNe are essential to understanding the chemical evolution of the Universe (Kobayashi et al. 2006; Andrews et al. 2017; Prantzos et al. 2018) and the injection of energy into the interstellar medium (ISM; Thornton et al. 1998). This local deposition of energy plays a crucial role in galaxy evolution, triggering star formation (Stinson et al. 2006; Dalla Vecchia & Schaye 2012; Hopkins et al. 2014) and seeding and sustaining turbulence (Mac Low & Klessen 2004).

Our understanding of the role that SNe play in the ecology of the ISM is limited by the many questions that remain open about their stellar progenitors. The baseline physical scenarios for the two major classes of SNe posit that core-collapse (CC) SNe arise from gravitational collapse in the cores of stars more massive than $\sim 8\,M_{\odot}$, and Type Ia SNe are the aftermath of a thermonuclear runaway ignited in the central regions of massive CO white dwarfs that are somehow destabilized by accretion in close binary systems. However, many important details of these scenarios remain obscure, including the roles played by binary interactions and pre-explosion progenitor mass loss in CCSNe (Smartt 2009; Smith 2014) and the specific identities of the progenitors in SNe Ia (Maoz et al. 2014). As a result, we have not been able to fully characterize fundamental properties that regulate the feedback mechanism into the ISM, like the distribution of progenitor masses and delay times (Badenes et al. 2009; Jennings et al. 2014; Zapartas et al. 2017; Auchettl et al. 2019; Strolger et al. 2020; Castrillo et al. 2021) or the detailed nucleosynthetic yields (Romano et al. 2010; Andrews et al. 2017).

Recent advances in astronomical instrumentation have opened new opportunities to explore these issues. In particular, the wide availability of data from integral field spectroscopy (IFS) makes it possible to study the properties of the host galaxies of SNe with an unprecedented level of detail, revealing a wealth of information about the environments in which SNe explode (e.g., Stanishev et al. 2012; Kuncarayakti et al. 2013a, 2013b, 2018; Rigault et al. 2013; Galbany et al. 2014, 2016a, 2016b, 2017, 2018; Krühler et al. 2017; Lyman et al. 2018, 2020; Rigault et al. 2018). Previous IFS studies of SNe have relied on dedicated SN surveys and literature searches to identify SN host galaxies and locate their explosion sites. Here, we describe the first results of an effort to use the IFS observations themselves to discover recent SNe. This is

possible because some SNe undergo strong interaction with a dense circumstellar medium (CSM) shortly after the explosion, leading to large luminosities that can be sustained for a long time (Milisavljevic & Fesen 2017; Dessart et al. 2023). These objects are often described as transitional, between SNe and Supernova Remnants (SNRs), and range from young SNe with clear evidence of CSM interaction, such as SN 1993J (Fransson et al. 1996; Matheson et al. 2000), SN1996cr (Bauer et al. 2008; Quirola-Vásquez et al. 2019), and SN 1978K (Kuncarayakti et al. 2016), to SNRs like Cas A, which remain optically bright centuries after the explosion (Milisavljevic et al. 2012). For clarity, we will refer to this class of objects as young SNRs. Our work is motivated by the fact that some of these young SNRs are luminous enough to stand out in narrowband images of their host galaxies (e.g., SNR NGC 4449; Milisavljevic & Fesen 2008) and in principle could be picked up serendipitously in IFS observations of nearby galaxies. To explore this possibility, we have conducted a systematic search for regions in IFS data cubes that are characterized by bright Hα line emission with a significant broad component ($\geqslant 400\,\mathrm{km\,s^{-1}}$) that could be associated with CSM interaction.

This paper is organized as follows. In Section 2, we describe the IFS data that constitute our initial sample. In Section 3, we outline the methods we have employed to identify candidate young SNRs. In Section 4, we discuss the main properties of our sample of young SNR candidates. In Section 5, we comment on our results and discuss possible avenues for future research.

2. Observations

Our initial sample is constituted by IFS observations of nearby galaxies obtained using two different instruments:

(i) the Potsdam Multi Aperture Spectrograph (PMAS; Roth et al. 2005) in PPak mode (Verheijen et al. 2004; Kelz et al. 2006), mounted on the 3.5 m telescope of the Centro Astronomico Hispano-Aleman at the Calar Alto Observatory. PPak consists of a fiber bundle of 382 fibers with 2.″7 diameter. Among these, 331 are ordered in a single hexagonal bundle, with the remaining fibers used for sky measurements and calibration purposes. Most objects are observed with two overlapping setups and then combined. The V500 grating has a spectral resolution of ∼6 Å in the wavelength range 3750–7300 Å. The V1200 grating has a higher spectral resolution of ∼2.7 Å, with a bluer range spanning 3400–4750 Å. The final products are 3D data cubes with a 100% covering factor within a hexagonal field of view (FOV) of $\sim$1.3 arcmin^2 with $1''\times1''$ pixels, which correspond to ∼4000 spectra per object.

(ii) the Multi-Unit Spectroscopic Explorer (MUSE; Bacon et al. 2014), located at the Nasmyth B focus of Yepun, the Very Large Telescope UT4 telescope at Cerro Paranal Observatory. It has a modular structure composed of 24 identical integral field unit modules that together sample, in wide-field mode, a near-contiguous 1 arcmin^2 FOV with spaxels of $0.''2\times0.''2$ and a wavelength coverage of 4650–9300 Å with a mean resolution of R ∼3000. MUSE produces ∼100,000 spectra per pointing.

Observations obtained with PMAS come in their majority from the third data release (DR) of the Calar Alto Legacy Integral Field Area (CALIFA) survey (Sánchez et al. 2012, 2016). The PMAS sample consists of 667 galaxies selected from DR7 of the Sloan Digital Sky Survey (Abazajian et al. 2009) with redshifts between 0.005 and 0.03, declinations $>-7°$, and diameters between 45″ and 79.″2. These selection criteria are optimized for the PMAS/PPak instrument. We added to this sample data from the PMAS/PPak Integral field Supernova hosts COmpilation (PISCO; Galbany et al. 2018), an extended project of CALIFA that aimed at increasing the sample of SN host galaxies used for environmental studies (Galbany et al. 2014, 2016b). As of 2020 January, the PISCO sample contained 220 galaxies, bringing the total PMAS sample to 887 galaxies.

Observations obtained with MUSE come in their totality from the All-weather MUse Supernova Integral-field of Nearby Galaxies (Galbany et al. 2016a; L. Galbany et al. 2024, in preparation.) survey. This survey has been running for 11 semesters (P95–P106) with the focus of obtaining IFS of SN host galaxies, each semester with a different science focus, including among others: the hosts of SNe that showed strong sodium absorption lines in their spectra, indicating the presence of large amounts of dust; the hosts of SNe discovered by the ASAS-SN survey, to study SN rates as a function of local environment (Pessi et al. 2023); SN hosts with low surface brightness (Holoien et al. 2023); and the hosts of SNe included in the Carnegie Supernova Project (Phillips et al. 2019) sample. The compilation used in this work consisted of 342 nearby SN host galaxies.

3. Detection Method

3.1. Pre-processing

All IFS data cubes are pre-processed in preparation for the analysis. First, regions with foreground stars are masked out. Then, single-stellar-population (SSP) synthesis models are fit to all individual spectra (around 4000 and 100,000 spectra per PMAS and MUSE cube, respectively) to separate the underlying stellar continuum from the ionized gas-phase emission. This is done with `STARLIGHT` (Cid Fernandes et al. 2005, 2009), which determines the fractional contribution of different SSP models to the spectrum, x_i, and to the galaxy mass, μ_i. `STARLIGHT` accounts for dust extinction (A_V^*) as a foreground screen, using a reddening law from Cardelli et al. (1989) that assumes $R_V = 3.1$. To reduce computing time, we used a reduced grid of 248 SSP models from Cid Fernandes et al. (2013), with 62 ages spanning 1 Myr–14 Gyr and four metallicities (0.2, 0.4, 1.0, and 1.5 solar). The best-fit model is subtracted from each observed spectrum and the resulting residual is stored in a 3D cube containing only the ionized gas-phase emission.

The resulting residual spectra are mostly flat, dominated by the narrow line emission from the host galaxy. We fit the most prominent lines (Hβ, [O III] λ5007, [O III] λ4969, [N II] $\lambda\lambda$ 6548,84, Hα, and [S II] $\lambda\lambda$ 6719,31) with the `Python` version of `MPFIT` (Markwardt 2009, 2012; Newville et al. 2016), which performs nonlinear least-squares fitting using the Levenberg–Marquardt minimization algorithm (Levenberg 1944; Marquardt 1963). For each residual spectrum, we focus on the wavelength range corresponding to each line and fit it using a Gaussian profile, to retrieve line fluxes, central wavelengths, velocity shifts and widths, and their corresponding errors. When required, more than one Gaussian is fitted

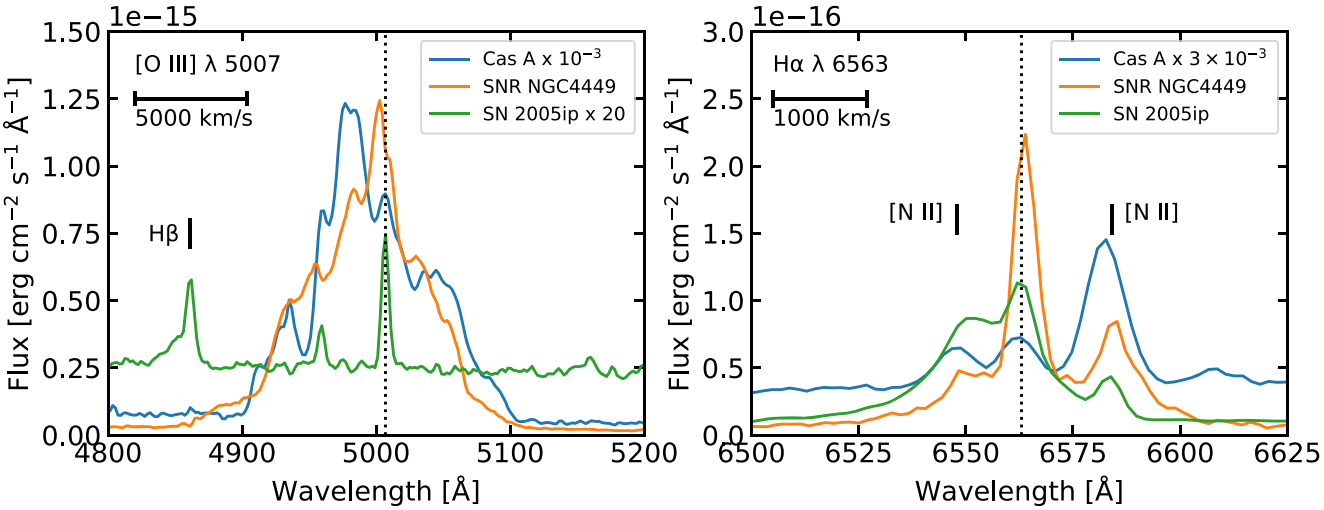

Figure 1. Optical spectra of Cas A and SNR NGC 4449 (both from Milisavljevic et al. 2012) and SN 2005ip (from our PMAS IFS data) around the [O III] λ5007 line (left) and the Hα line (right).

simultaneously for transitions that are close to one another (Hα with the two [N II], the two [S II], and Hβ with [O III]).

We correct all the fitted line fluxes for reddening intrinsic to the host galaxy by measuring the Hα to Hβ ratio and applying an extinction law from Cardelli et al. (1989), assuming $R_V = 3.1$, Case B recombination, and densities of $\sim 10^3$ cm^{-3} around a heating source with $T \sim 10^4$ K and a large optical depth (Osterbrock & Ferland 2006). We note that the extinction correction and the selection of a particular extinction law do not affect the method we use to detect young SNR candidates.

3.2. Line Emission from Young SNRs in IFS Data: An Illustrative Example

Young SNRs have distinctive optical spectra. In Figure 1, we show the integrated line emission in two spectral windows around the [O III] λ5007 and Hα lines from the Galactic SNR Cas A (age $\sim$340 yr; Thorstensen et al. 2001; Milisavljevic et al. 2012), the SNR in NGC 4449 (age $\sim$80 yr; Milisavljevic & Fesen 2008; Bietenholz et al. 2010), and SN 2005ip (age $\sim$17 yr), which we use as an illustrative example of a young SNR imaged by our IFS data. SN 2005ip is a bright, well-observed Type IIn SN that exploded in NGC 2906 (Fox et al. 2009, 2010) and has been showing signs of strong CSM interaction and enhanced dust formation for well over a decade (Smith et al. 2009, 2017; Stritzinger et al. 2012; Katsuda et al. 2014; Bevan et al. 2019; Fox et al. 2020). All three objects show bright emission in both lines, with Cas A and SNR NGC 4449 being brighter in [O III] and SN 2005ip being brighter in Hα. The Hα emission is noticeably broadened by several hundred kilometers per second due to shock interactions in all three objects, although in all cases this broad emission appears superimposed on several components of narrow emission from Hα and the neighboring [N II] $\lambda\lambda$ 6548,84 doublet. The [O III] λ5007 line is broadened by several thousand kilometers per second in both Cas A and SNR NGC 4449, but the spectrum from SN 2005ip appears much narrower, even if the neighboring Hβ line has a clear blueshifted broad component.

A detailed physical interpretation of the line emission from young SNRs is outside the scope of the present work. In particular, the mapping between shock physics and line emission is likely to be complex—we note that our IFS data only provide an unresolved view of objects that probably have a great deal of spatial structure, which can only be studied in detail in nearby cases like Cas A (Milisavljevic et al. 2012; Milisavljevic & Fesen 2015). We refer the reader to Fransson et al. (2002) and Milisavljevic et al. (2012) for further details. For our purposes, the qualitative comparisons shown in Figure 1 are enough to illustrate the ability of IFS data cubes to recover young SNe with strong CSM interaction.

Detailed fits to the line emission from the PMAS and MUSE residual spectra around Hα at the location of SN 2005ip are shown in Figure 2. The default fits to the narrow line emission from the host galaxy are shown in the right panels. The three narrow Gaussians for Hα and the [N II] doublet emission miss much of the measured flux, and try to compensate for this by overfitting the [N II] line at $\lambda = 6548$ Å, resulting in an unphysical flux ratio for the [N II] doublet. The addition of a fourth Gaussian corresponding to a broad Hα component associated with SN 2005ip greatly improves the spectral fit, accounting for all the observed flux and recovering the correct flux ratio for the narrow component of the [N II] doublet. The width of this component in the IFS data cubes is $\sigma_{\rm PMAS} = 14.41 \pm 5.92$ Å and $\sigma_{\rm MUSE} = 12.31 \pm 3.26$ Å, which correspond to FWHM velocities of 1550 ± 637 and 1324 ± 351 km s^{-1}, respectively.

To evaluate our IFS observations of SN 2005ip in context, we have compiled the 30 single-slit spectra of the SN analyzed by Smith et al. (2009) and Smith et al. (2017), which span ages between 17 days and more than 10 yr after discovery. As noted in these references, the broad Hα emission from SN 2005ip has at least two components, which evolve in distinct ways (see e.g., Figure 5 in Smith et al. 2009). In Table 1, we list the fitted FWHM values for these two components, which we have labeled "broad" and "intermediate," in the single-slit spectra of SN 2005ip. The overall temporal evolution of these FWHM values is shown in Figure 3, together with our IFS observations. The broadest of the two components is only seen clearly in spectra taken before 2006 April (MJD 53852 or 172 days after discovery; see Table 1), but the intermediate component is always present. The evolution of the broad component shows an initial free expansion ($v \sim$ ct) phase, with a clear transition to a Sedov regime ($v \propto t^{-3/5}$) approximately 60 days after the

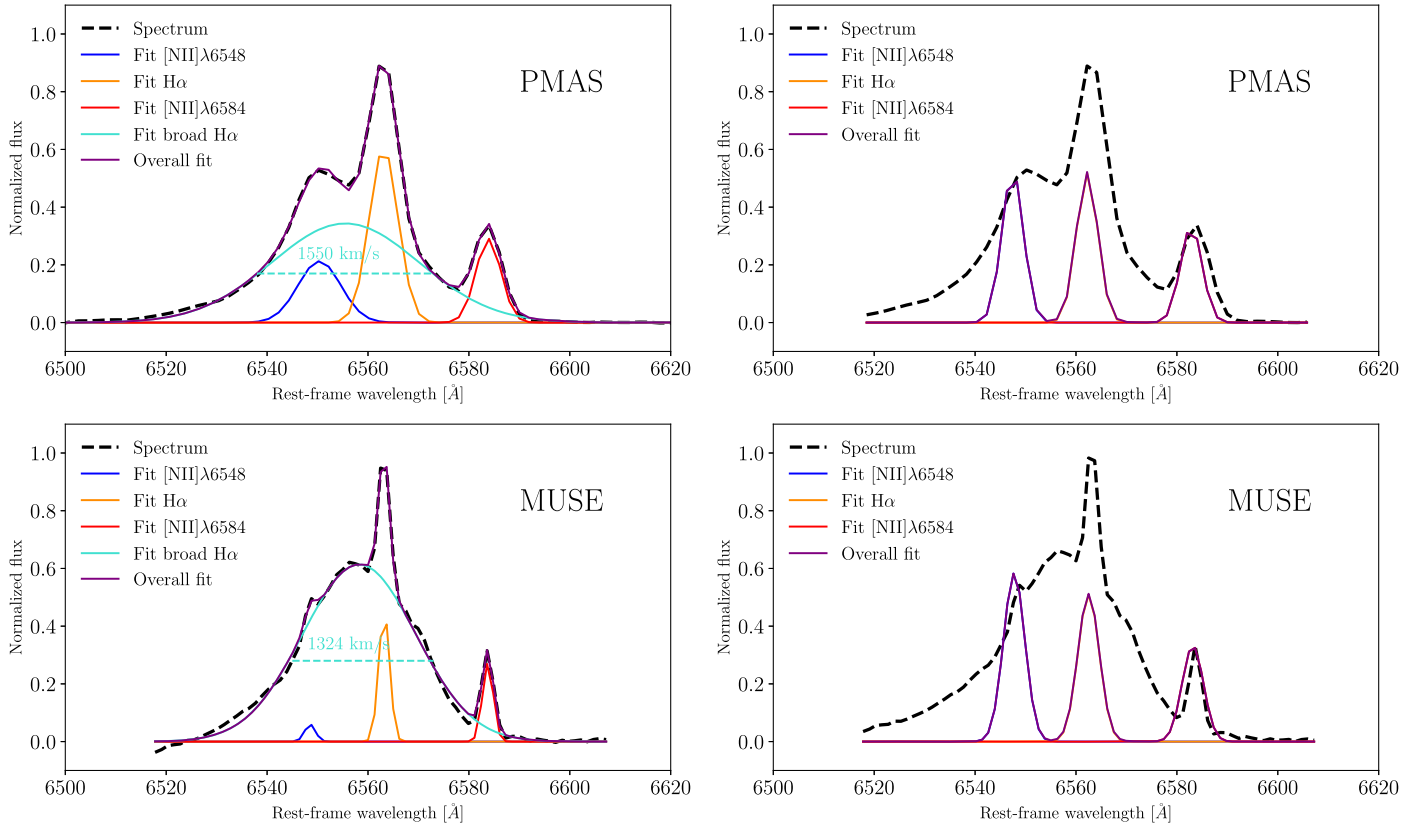

Figure 2. Left: line fits to the residual spectrum of NGC 2906 at the location of SN 2005ip in PMAS (top) and MUSE (bottom). The blue, red, and orange lines show the narrow [N II] doublet and Hα, while the turquoise line shows the broad Hα component corresponding to SN 2005ip. This broad component is blueshifted with respect to the narrow Hα emission from the host galaxy. The FWHM of the Hα emission from SN 2005ip is shown as the horizontal dashed line. The overall fit and emission spectrum are shown with the purple and black dashed lines, respectively. Right: the same residual spectra as shown in the left panels, fitted without including the broad Hα component. Notice the inability of the fitted narrow line emission (purple line) to reproduce the observed residual spectrum (dashed black line).

explosion. This early transition to a Sedov regime, which happened while the SN was still optically bright, is consistent with the hypothesis that the SN progenitor lost a large amount of mass shortly before the explosion (see Moriya et al. 2013 for a discussion). The intermediate component, on the other hand, shows a slower deceleration, roughly as $v \propto t^{-1/7}$. The physical interpretation for the behavior of the intermediate component is less clear, but we emphasize that our IFS measurements are broadly consistent with those obtained from contemporary single-slit spectra, showcasing the ability of galaxy-wide IFS data sets to study bright young SNRs and obtain physically meaningful measurements from them.

The broad component to the Hα emission associated with SN 2005ip does not appear at any other location in the IFS data cubes for the host galaxy NGC 2906. To illustrate this, we added a broad emission component to the fits to the residual spectra in the Hα region for all spaxels, in addition to the narrow Hα and the two narrow [N II] lines. This broad component has a minimum width of 400 km s^{-1}, but no minimum amplitude, so that MPFIT returns a zero value for the amplitude when the spectral fit does not require it. For the remainder of the paper, we will not distinguish between "broad" and "intermediate" components to the Hα line emission, as defined in the case of SN 2005ip, but will use the notation "broad" to describe any contribution to the line flux that is clearly broader than usual (i.e., that is not kinematically narrow). Figure 4 shows the flux maps for NGC 2906 generated by this procedure for both the narrow (left column) and broad (right column) Hα components, in the PMAS (top row) and MUSE (bottom row) data. The narrow component is distributed throughout the entire disk of the galaxy, showcasing emission from individual H II regions, but the broad component is restricted exclusively to the location of SN 2005ip. Note how the higher spatial resolution of MUSE (0.″2 compared to 1″ for PMAS) allows us to accurately pinpoint the site of the SN.

Without spatial coincidence with a previously recorded SN, as seen here for SN 2005ip, it is impossible to determine with absolute confidence that a region showing broad line emission in an IFS data cube is in fact a young SNR. In general, broad line emission in IFS data cubes is often associated with active galactic nuclei in the central regions (see, e.g., Papaderos et al. 2013; Singh et al. 2013; Lacerda et al. 2020). Off-center broad line emission has been associated with sources like stellar outflows from supergiants or Wolf–Rayet clusters (e.g., Diaz et al. 1987; Terlevichet al. 1991; Kehrig et al. 2020), but the vast majority of these examples have low luminosities, which would be hard to disentangle from the background in IFS data cubes, and modest widths, with FWHMs below 200 km s^{-1}. In rare cases, bright Hα emission with FWHM in excess of 1000 km s^{-1} has been reported in single-slit spectra, like the giant H II region NGC 5471 in M101 (Castaneda et al. 1990). For this specific example, follow-up X-ray observations indicate the presence of at least one SNR at this location (Williams & Chu 1995). Of course, larger-scale ionized flows outflows have been found in starburst and post-starburst galaxies like the "green peas" (Amorín et al. 2012; Rodríguez Del Pino et al. 2019; Hogarth et al. 2020), but these outflows

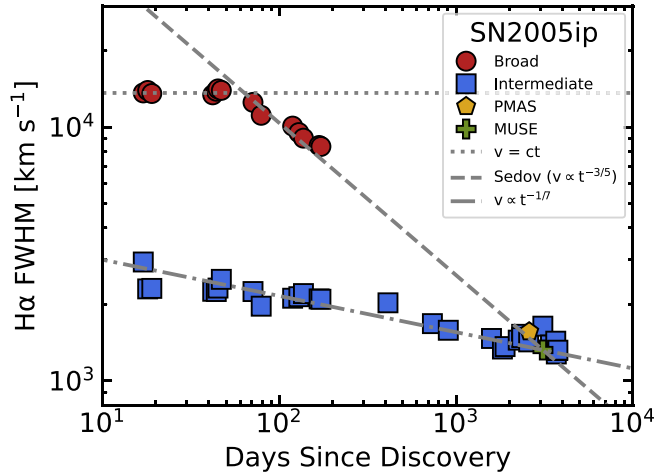

Figure 3. Temporal evolution of the FWHM for the two components of the Hα emission from SN 2005ip, calculated from the spectra analyzed in Smith et al. (2009) and Smith et al. (2017; red circles for the broad component and blue squares for the intermediate component), together with the IFS observations from PMAS and MUSE shown in Figure 2 (yellow pentagon and green cross). Three lines are included for illustrative purposes: a constant velocity set to the FWHM of the broad component in the first spectrum ($t = 17$ days), a Sedov solution ($v \propto t^{-3/5}$) anchored to the FWHM of the MUSE spectrum, and a $v \propto t^{-1/7}$ power law, also anchored to the FWHM of the MUSE spectrum.

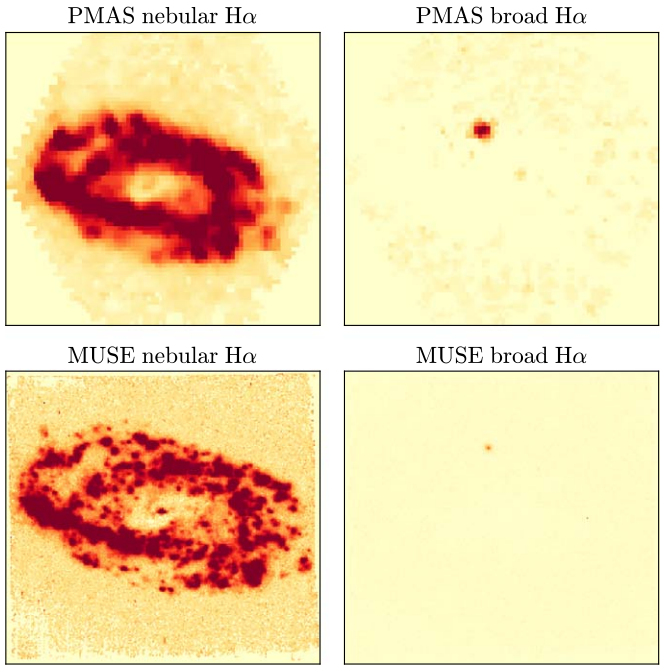

Figure 4. Hα flux maps for NGC 2906. The Hα contribution from SN 2005ip (right) can be separated from that of its host galaxy (left). Top: PMAS. Bottom: MUSE.

will not appear as high-contrast point sources like the IFS detection of SN 2005ip shown in Figure 4.

4. A Systematic Search for Young SNRs in IFS Data

4.1. Search Method

The illustrative example of SN 2005ip demonstrates that IFS data cubes have the potential to both recover emission from young SNRs and extract relevant physical information about them. Motivated by this realization, we have conducted a systematic search for broad Hα emission in all the IFS data of all the nearby galaxies in our sample. To do this, we defined a set of criteria designed to single out young SNR candidates without making strong assumptions about the specific properties of their line emission. First, we require a minimum FWHM of 400 km s^{-1}, which should be enough to remove most non-SN local outflows. Second, we use the flux (F), flux uncertainty (ΔF), width (σ), and width uncertainty ($\Delta\sigma$) of the Gaussian fits to the broad Hα component (denoted as Hα, SNR) to define two diagnostic ratios designed to single out bright line emission from young SNR candidates:

1. $\log(\sigma_{\mathrm{H}\alpha,\mathrm{SNR}}/\Delta\sigma_{\mathrm{H}\alpha,\mathrm{SNR}})$;
2. $\log(F^2_{\mathrm{H}\alpha,\mathrm{SNR}}/\Delta F_{\mathrm{H}\alpha,\mathrm{SNR}})$.

We show the values for these two diagnostic ratios in all the spaxels of the MUSE data cube for NGC 2906 in Figure 5. This plot illustrates the discriminating power of our chosen diagnostic ratios, with the spaxels that cover the site of SN 2005ip clearly deviating from the distribution of values measured in the rest of the host galaxy along both axes.

We have examined the values of these diagnostic ratios in all IFS data cubes in our sample of 887 PMAS and 342 MUSE observations of nearby galaxies, consisting of more than 35 million individual spectra. To minimize false detections, we restrict our search to spaxels where the signal-to-noise ratio

Table 1
FWHMs of the Two Components, Broad and Intermediate, of SN 2005ip Measured in Spectra Obtained from the Literature Plus our PMAS and MUSE Measurements

Date MJD	$\mathrm{FWHM_{Broad}}$ (km s^{-1})	$\mathrm{FWHM_{Intermediate}}$ (km s^{-1})
53697	13625.0 ± 1899.9	2936.1 ± 1982.2
53698	13936.1 ± 2031.7	2299.7 ± 1302.9
53699	13556.2 ± 1865.8	2310.0 ± 1218.9
53722	13393.3 ± 1891.5	2250.6 ± 1360.3
53724	13841.3 ± 2005.5	2245.7 ± 1399.2
53725	14133.7 ± 1994.1	2317.4 ± 1472.2
53727	13947.9 ± 1910.5	2508.1 ± 1663.6
53751	12507.7 ± 1544.1	2245.2 ± 1128.8
53759	11121.5 ± 1325.6	1965.7 ± 714.0
53799	10085.8 ± 1587.2	2113.0 ± 848.7
53809	9507.8 ± 538.9	2142.5 ± 525.7
53817	9037.8 ± 670.6	2204.2 ± 670.6
53848	8458.0 ± 681.1	2099.8 ± 681.1
53852	8272.0 ± 703.5	2093.0 ± 488.3
54092	⋯	2026.7 ± 339.4
54415	⋯	1677.9 ± 364.9
54584	⋯	1579.7 ± 302.2
55267	⋯	1466.1 ± 331.9
55510	⋯	1332.2 ± 342.5
55574	⋯	1361.9 ± 264.4
55928	⋯	1444.0 ± 328.0
56030	⋯	1522.7 ± 379.8
56033	⋯	1477.5 ± 351.7
56255	⋯	1421.3 ± 262.1
56273	⋯	1559.6 ± 636.9
56778	⋯	1639.7 ± 392.9
56783	⋯	1320.4 ± 350.6
57103	⋯	1381.5 ± 321.0
57346	⋯	1430.7 ± 352.9
57372	⋯	1273.6 ± 238.6
57433	⋯	1314.2 ± 262.8
57449	⋯	1318.3 ± 310.4

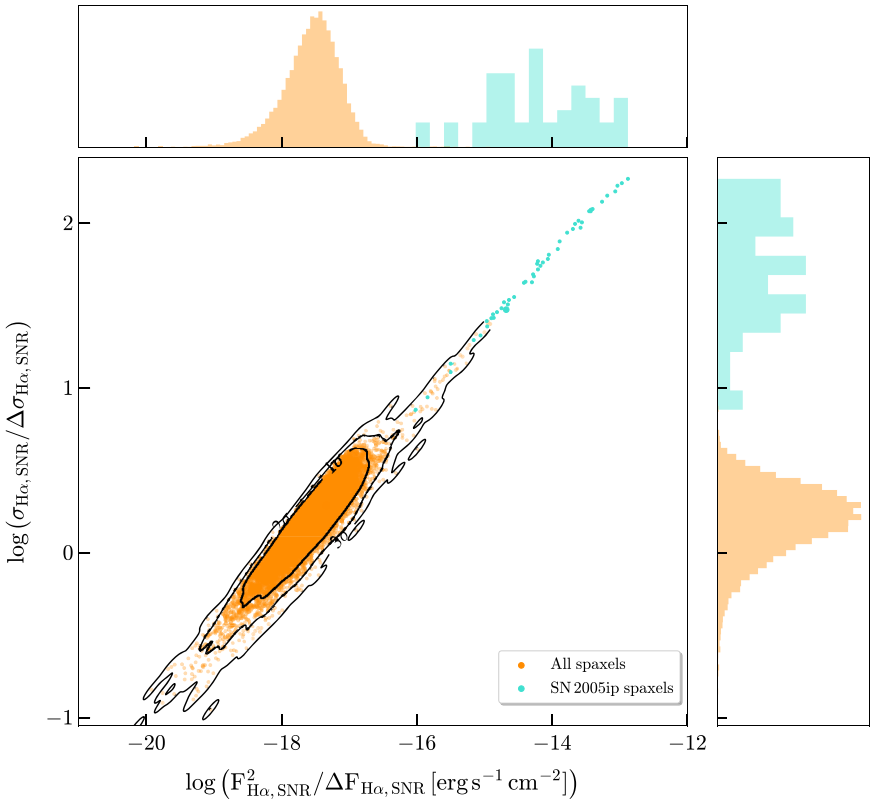

Figure 5. Diagnostic plot showing the MUSE data for the entire galaxy NGC 2906. F, ΔF, σ, and $\Delta\sigma$ represent the fluxes and widths of the broad components in the Hα line with their uncertainties. Spaxels where the broad Hα component was detected are shown in turquoise, while the rest of the spaxels in the galaxy are shown in orange. The black contours indicate the 1σ, 2σ, and 3σ confidence contours of the distribution of each quantity.

Table 2
Coordinates, Broad Hα Fluxes, and Luminosities of the 20 SNR Candidate Regions with Broad Hα Emission

Host Galaxy	Redshift	Survey	R.A. J2000	decl. J2000	$v_{H\alpha,SNR}$ (km s^{-1})	$FWHM_{H\alpha,SNR}$ (km s^{-1})	$L_{H\alpha,SNR}$ (10^{36} erg s^{-1})
LEDA 43070[a]	0.0158	MUSE	12:46:14.75	−40:48:52.59	141 ± 63	1932 ± 547	3.159 ± 0.760
2MASX J23331223-6034201	0.0148	MUSE	23:33:10.63	−60:34:29.87	103 ± 86	442 ± 216	1.206 ± 0.212
LEDA 1015413	0.0131	MUSE	12:54:12.58	−07:38:37.19	161 ± 62	503 ± 358	10.811 ± 2.018
NGC 2906[b]	0.0074	MUSE	09:32:06.42	+08:26:44.53	−258 ± 53	1325 ± 350	7.720 ± 0.806
NGC 4806[c]	0.0082	MUSE	12:56:14.02	−29:29:54.74	−11 ± 51	953 ± 358	7.551 ± 1.891
ESO 467-51[d]	0.0060	MUSE	22:23:16.15	−28:58:31.17	288 ± 90	1551 ± 299	7.045 ± 1.023
NGC 1448	0.0037	MUSE	03:44:30.39	−44:38:50.48	157 ± 25	1504 ± 485	0.290 ± 0.046
Arp 142	0.0233	PMAS	09:37:42.50	+02:45:26.76	−226 ± 73	415 ± 209	29.628 ± 7.400
MCG +11-08-25	0.0136	PMAS	06:15:48.81	+66:50:21.60	174 ± 68	1271 ± 386	5.933 ± 1.744
NGC 1056	0.0052	PMAS	02:42:47.98	+28:34:27.41	286 ± 23	1661 ± 489	0.398 ± 0.055
NGC 2276	0.0081	PMAS	07:27:07.12	+85:44:35.71	−411 ± 78	411 ± 261	1.327 ± 0.264
NGC 2906[b]	0.0074	PMAS	09:32:06.47	+08:26:44.94	−334 ± 42	1552 ± 638	4.2513 ± 0.510
NGC 5633	0.0078	PMAS	14:27:27.69	+46:08:36.14	−201 ± 84	414 ± 206	1.579 ± 0.179
NGC 5735	0.0125	PMAS	14:42:34.95	+28:43:38.18	−284 ± 78	439 ± 199	4.997 ± 0.590
NGC 5908[e]	0.0110	PMAS	15:16:42.08	+55:24:59.85	679 ± 79	3423 ± 713	1.020 ± 0.156
NGC 6946	0.0001	PMAS	20:34:51.87	+60:12:52.70	−163 ± 76	480 ± 276	0.001 ± 0.001
UGC 04179	0.0186	PMAS	08:02:07.59	+00:48:27.79	−581 ± 61	1486 ± 551	20.501 ± 7.007
UGC 09110	0.0156	PMAS	14:14:12.55	+15:37:04.78	501 ± 20	1311 ± 421	2.372 ± 0.255
UGC 09182	0.0155	PMAS	14:20:45.95	+21:56:16.12	−199 ± 34	401 ± 121	14.092 ± 8.745
MCG +03-31-094	0.0030	PMAS	12:17:26.07	+17:39:16.06	−59 ± 91	1360 ± 343	0.109 ± 0.012

Notes.
[a] ASAS-SN 14fd (Holoien et al. 2019).
[b] SN 2005ip (Fox et al. 2009; Smith et al. 2009).
[c] SN2011fh (Pessi et al. 2022).
[d] ASAS-SN 14jb (Holoien et al. 2019).
[e] Coincides with the SN impostor reported in 2012, PSNJ15164204+5525011 (Benetti et al. 2012).

(S/N) for Hα, SNR is higher than 5 in the residual spectra. We have set a conservative threshold of 3σ above the median of the distribution in both diagnostic ratios to flag regions of interest as young SNR candidates.

As a side note, we attempted a similar search centered on the [O III] λ5007 line, but we failed to find any clear candidates. This indicates that objects with strong, broad [O III] emission, like Cas A and SNR NGC 4449 (Figure 1), must be rare, or short-lived, or both.

4.2. Young SNR Candidates

Our search yielded 20 contiguous regions that pass our quality cuts, seven in MUSE and 13 in PMAS. We list these regions in Table 2 and classify them as young SNR candidates, by analogy with the properties of SN 2005ip described in Section 3.2. The only object that appears in both the MUSE and PMAS data is SN 2005ip itself, which brings the total number of unique objects identified in our search to 19. The individual fits to the residual spectra around Hα in the spaxels identified as young SNR candidates are shown in Figures 6, 7, and 8, along with maps of the entire host galaxy, both in the broad Hα component and in white light. The regions outside the SNR candidates that appear in some of these broad Hα maps did not pass our quality cuts. In Figure 9, we show the distribution of the host galaxy redshifts, along with the FWHM, luminosity, and systemic velocity of the broad Hα component corresponding to these regions.

Four of these 19 objects coincide spatially with previously known SNe: the already discussed SN 2005ip, a Type IIn SN in the spiral NGC 2906 imaged by PMAS and MUSE 2593 and 3104 days after discovery, respectively; ASAS-SN 14fd (Holoien et al. 2019), a Type IIn SN in the dwarf irregular galaxy LEDA 43070 (PGC 43070) imaged by MUSE 514 days after discovery; SN2011fh (Pessi et al. 2022), a Type IIn SN in the spiral NGC 4806 imaged by MUSE 1362 days after discovery; and ASAS-SN 14jb (Holoien et al. 2019), a Type IIP SN in the spiral ESO 467-51 imaged by MUSE 391 days after discovery. A fifth object, the SNR candidate in NGC 5908, coincides spatially with PSNJ15164204+5525011, an "SN impostor" reported in 2012, likely a luminous blue variable (Benetti et al. 2012).

It is worth noting that three out of four SNe that coincide with our SNR candidates are Type IIn, despite the fact that this subtype only accounts for ~9% of CCSNe (Smith et al. 2011; Kiewe et al. 2012). The fourth SN, ASAS-SN 14jb, is a rare extraplanar Type IIP SN in an edge-on spiral, whose MUSE observations were analyzed and discussed in Meza et al. (2019). The remaining 15 candidates in our sample are probably young SNRs whose SNe either exploded before the era of modern transient surveys or were missed, perhaps because of weather, or poor sampling, or coincidence with the Sun. With distances up to ~100 Mpc (for SNR Arp 142, at a redshift of 0.0233; see Figure 9), these are among the farthest SNRs identified as such. Interestingly, one of our candidate SNRs is located in NGC 6946, the "Fireworks Galaxy," a nearby spiral with a high star formation rate that has hosted 10 known SNe (Eldridge & Xiao 2019; Eibensteiner et al. 2022). Our results bring the total number of SNe in this galaxy up to 11.

With all the caveats attached to small number statistics, the four objects associated with known SNe in our sample suggest that our method is turning up SNRs whose Hα luminosity is driven predominantly by CSM interaction, likely CCSNe whose progenitors have lost a great deal of mass in their pre-SN evolution, either due to winds or binary interactions (Smith et al. 2009; Langer 2012; Dessart et al. 2023). Some (possibly most) of these SNe might have shown signs of interaction during their optically thick phase, appearing as Type IIn or Type Ibn SNe (Kiewe et al. 2012; Taddia et al. 2013; Smith 2017). Others, like ASAS-SN 14jb, might not have developed those signs until later on, particularly if the progenitor drove some sort of fast outflow, clearing a low-density cavity surrounded by denser and slower material (Dwarkadas 2005, 2007; Patnaude et al. 2015, 2017). There is of course no way to tell how old these SNRs might be, but given the properties of Cas A, SNR NGC 4449, and SN2005 ip discussed in Section 3.2, ages ranging between a few years and a few centuries seem reasonable.

Eight of our young SNR candidates have FWHM values that are within 25% of our lower threshold of 400 km s^{-1}: 2MASX J23331223-6034201, LEDA 1015413, Arp 142, NGC 2276B, NGC 5735, NGC 6946, and UGC 09182. While these candidates might be considered somewhat more marginal than the others, it is important to emphasize that in each case the fit to the Hα spectral window does require the presence of a broad component with a high level of significance that shows spatial clustering in the 2D maps. The FWHM values in the other 11 candidates range between 953 ± 358 km s^{-1} for NGC 4806/SN2011fh and 3423 ± 713 km s^{-1} for NGC 5908, comparable to the values measured in X-ray-bright SNRs decades to centuries after the SN explosion (Vink 2012). We note that the errors produced by MPFIT for the FWHMs and systemic velocities of the broad Hα component are likely underestimated in the SNR candidates with the largest FWHM values. A Bayesian analysis might reveal substantial correlations in the posterior distributions for these parameters, but that is outside the scope of the present work. With one exception, the luminosities we measure for the broad Hα component in our SNR candidates range between 3×10^{35} and 3×10^{37} erg s^{-1}. The outlier, with a luminosity of 9×10^{32} erg s^{-1}, is the SNR candidate in NGC 6946, which is also by far the closest galaxy in our sample (7.9 ± 4.0 Mpc; Eldridge & Xiao 2019). For comparison, the Hα luminosities of the 143 SNRs in five nearby galaxies compiled by de Grijs et al. (2000) range between 10^{36} and 10^{38} erg s^{-1} (see Figure 9). Although there is considerable overlap in these luminosity ranges, it is important to keep in mind that all our SNR candidates show considerably broad emission, while most local SNRs (including those in the sample from de Grijs et al. 2000) do not.

In Figure 10, we show the distributions of the metallicities, star formation rates, and average stellar ages of the candidate SNRs in our sample, derived from the IFS spectra at their locations, compared to larger samples of CC and Type Ia SNe from PISCO (190 CCSNe and 234 SN Ia, respectively; Galbany et al. 2018). All the parameters for our SNR candidates have been measured following the procedures described in Galbany et al. (2018). The metallicities at the locations of the candidate SNRs are somewhat lower than those found in the environments of the PISCO CCSNe, and the star formation rates are intermediate between the CC and Ia SNe in the PISCO samples, but these differences are small and hard to interpret for a sample as small as ours. The most striking systematic difference between our candidate SNRs and the bulk population of PISCO SNe is in the average stellar ages, which

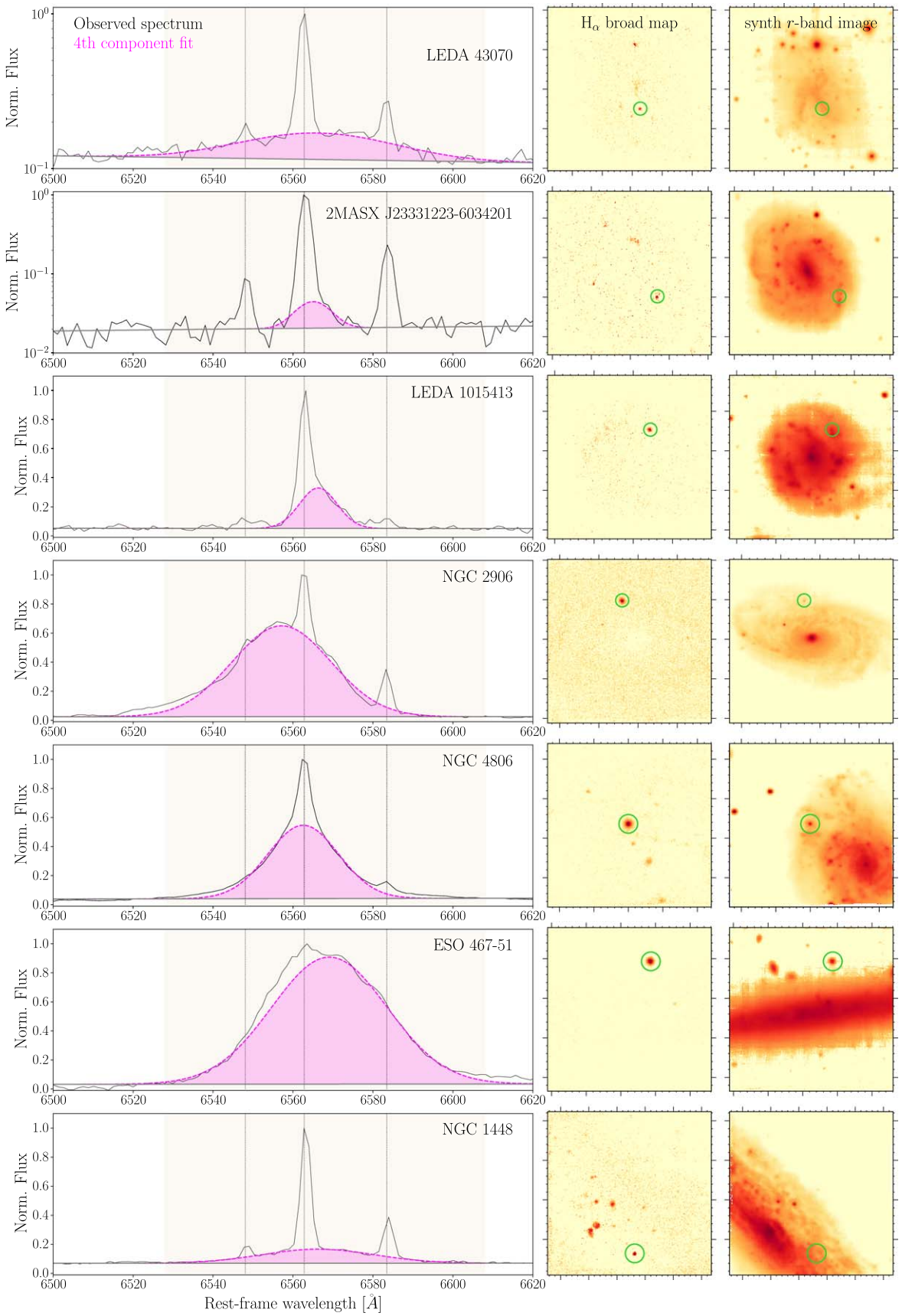

Figure 6. Left: spectra of young SNRs identified in our IFS sample in the Hα region, with the broad Hα component highlighted in magenta. Middle: spatial distribution of the broad Hα component in the entire footprint of the IFS data. Right: image of the IFS data footprint in white light.

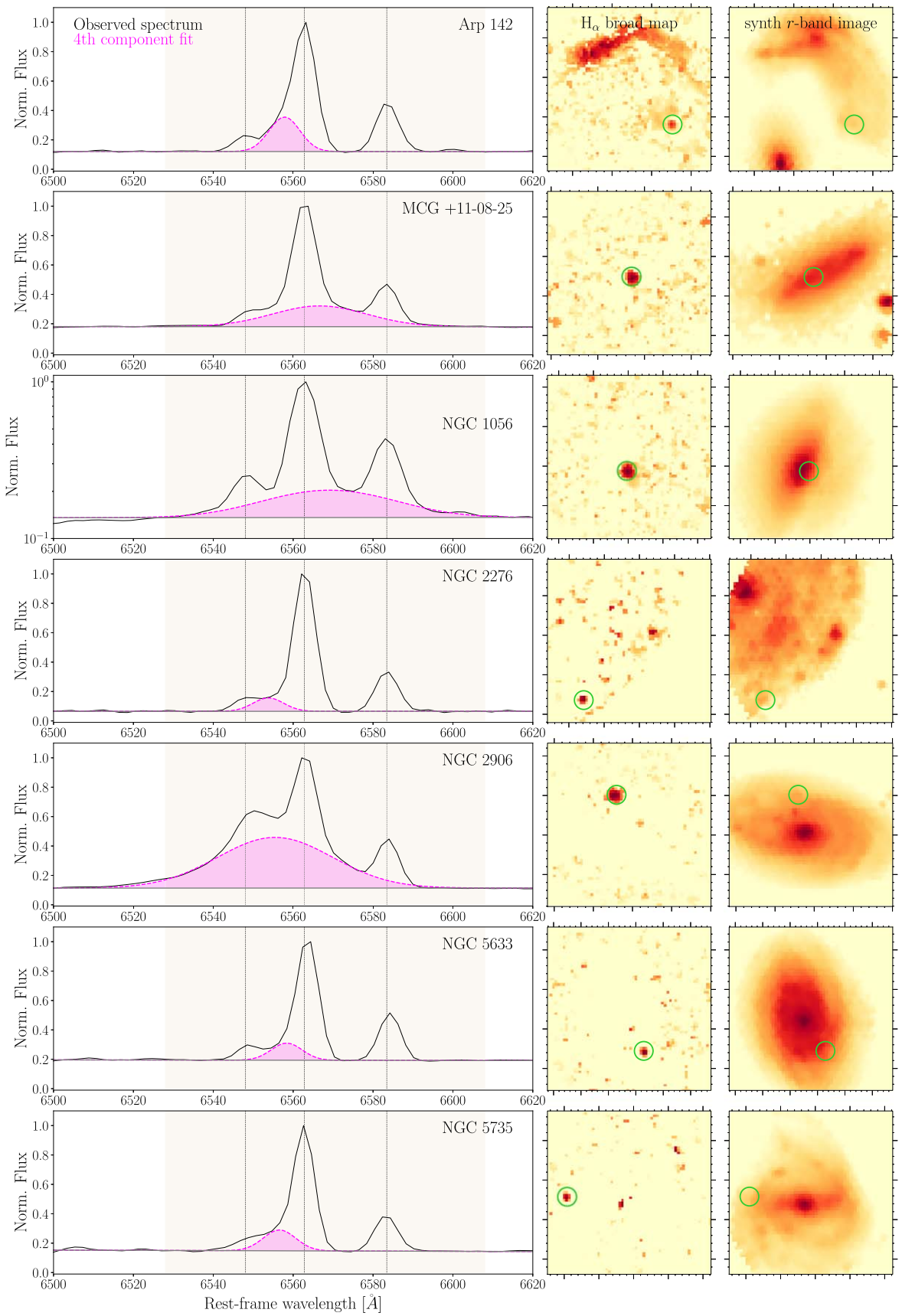

Figure 7. The same as Figure 6.

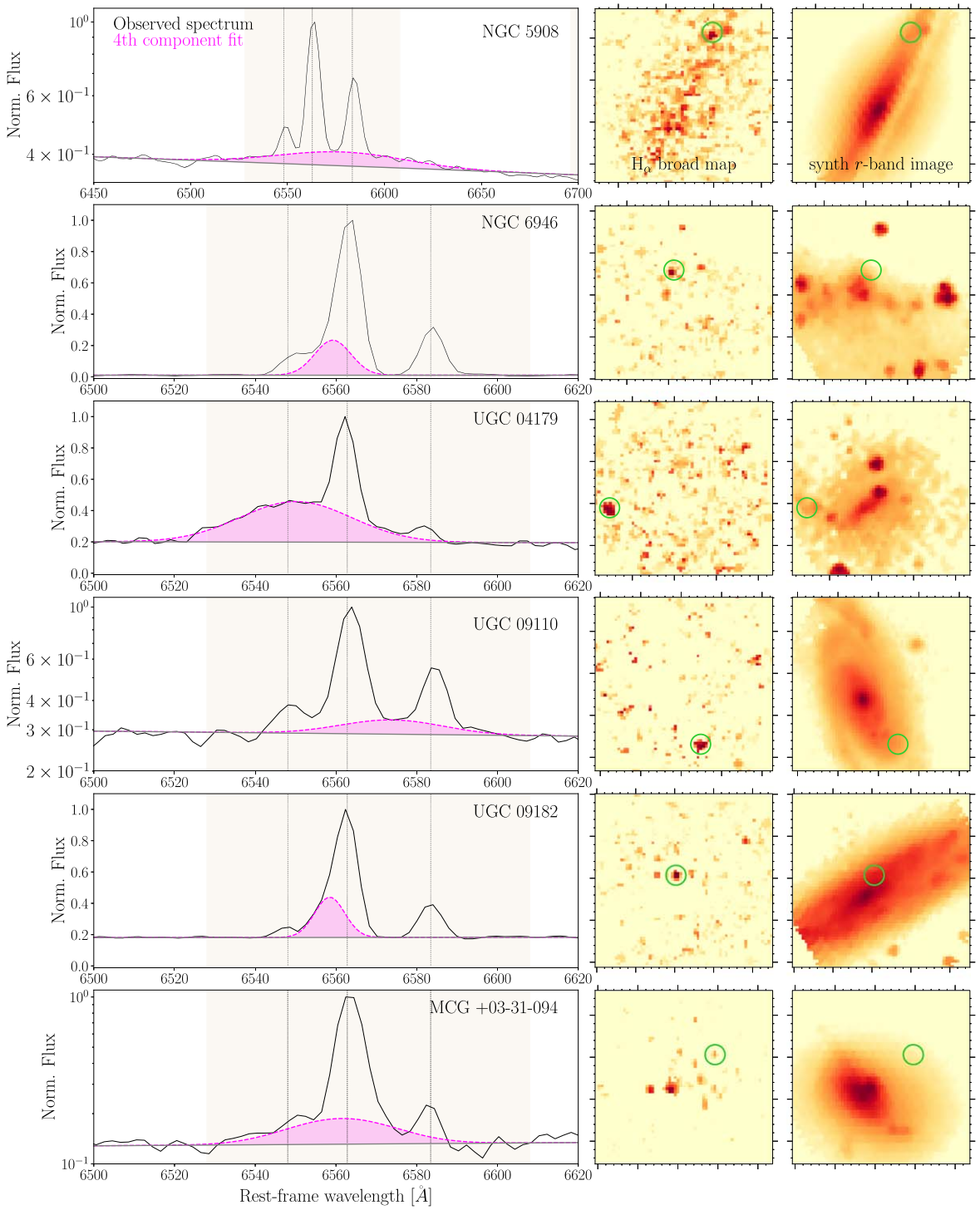

Figure 8. The same as Figure 6.

are clearly lower by about half a dex than those found in the environments of CCSNe, and about a dex lower than those of SN Ia. This indicates that the progenitors of our candidate SNRs might be shorter lived, and hence more massive, than those of a typical CCSNe. A similar trend has been found for the environments of Type IIn SNe by Moriya et al. (2023).

5. Discussion and Conclusions

We have conducted a systematic search for regions with broad ($\geqslant$400 km s^{-1}) Hα emission in IFS data cubes of 1229 nearby galaxies imaged by the PMAS and MUSE instruments. We have identified 19 such regions, which we classify as SNR candidates, by analogy with the properties of known objects like Cas A and SNR NGC 4449-1. Indeed, four of the regions we have found coincide with the sites of previously known CCSNe, one Type IIP and three Type IIn, including the well-known interacting object SN 2005ip. These coincidences, and the physical properties of the SNR candidates we have identified, suggest that the broad Hα emission in these regions is produced by a strong interaction between SN ejecta and

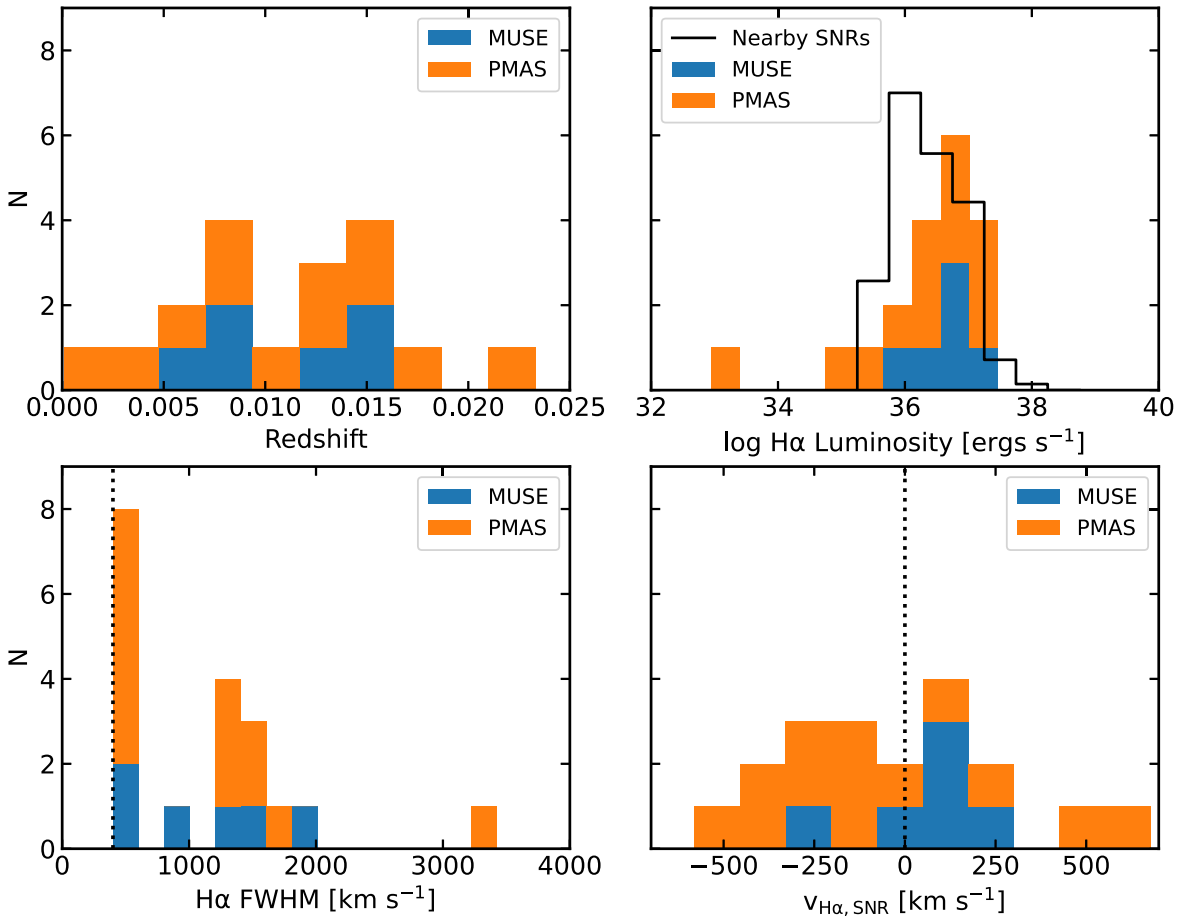

Figure 9. Histograms of host redshift (top left), Hα luminosity (top right), Hα FWHM (bottom left), and Hα systemic velocity (bottom right) for the young SNR candidates in our sample. The histogram of Hα luminosities in the sample of 143 SNRs in nearby galaxies compiled by de Grijs et al. (2000) is superimposed on the top left panel, scaled down by a factor 7 for comparison. The lower limit to the Hα FWHM in our fits (400 km s^{-1}) is indicated by a vertical dotted line in the bottom left panel.

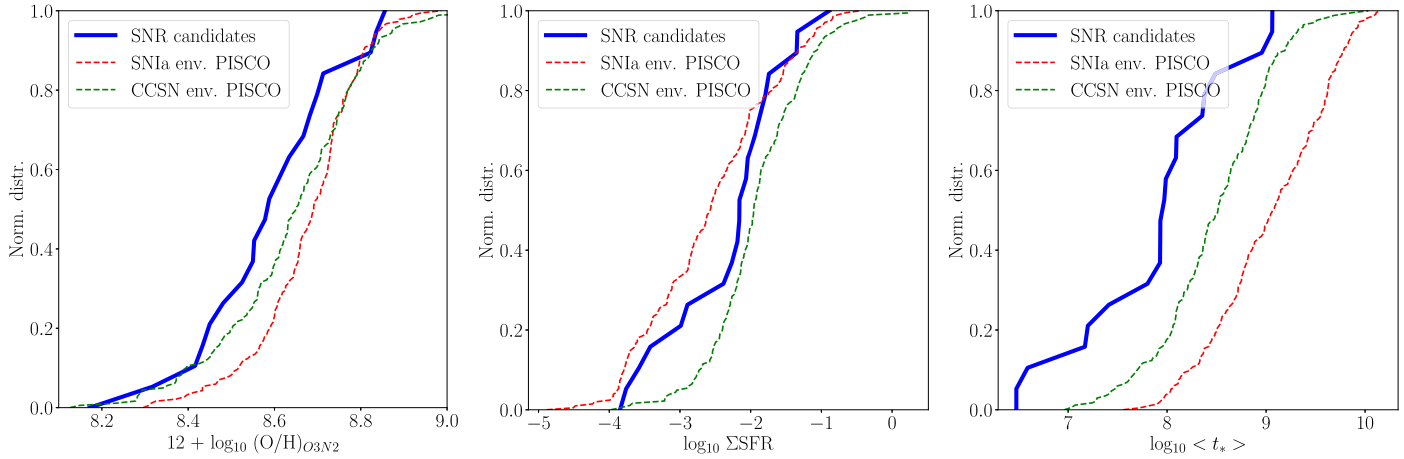

Figure 10. Distributions of oxygen abundance using the O3N2 calibration from Pettini & Pagel (2004), star formation rate density (within 1 sq. kpc), and average stellar age for the regions of interest compared to the same parameters from all SNe Ia and CCSNe from the PISCO sample (Galbany et al. 2018).

some sort of dense surrounding medium. This medium could be material lost by the SN progenitor before the explosion, due to stellar winds or binary interactions, which seems to be a common feature in Type IIn SNe, or a dense component of the ISM associated with the formation site of the SN progenitors. The stellar ages measured from the IFS data at the sites of our SNR candidates are younger by about 0.5 dex than the ages measured at the sites of Type II SNe in the PISCO survey, indicating that the progenitors of our SNR candidates might be more massive than those of average CCSNe.

The methods presented in this paper open a new window for the study of young SNRs in nearby galaxies. Systematic searches

for broad line emission in IFS data cubes in current and future surveys should yield more SNR candidates like the ones we present here, and allow us to study their progenitor population in greater detail.

Acknowledgments

We acknowledge useful discussions with Sedona Price and Evan Schneider. H.M.-R. and C.B. are funded by the NASA ADAP grant NNX15AM03G S01. H.M.-R. also acknowledges support from a PITT PACC, a Zaccheus Daniel and a Kenneth P. Dietrich School of Arts & Sciences Predoctoral Fellowship. L.G. acknowledges financial support from the Spanish Ministerio de Ciencia e Innovación (MCIN), the Agencia Estatal de Investigación (AEI) 10.13039/501100011033, the European Social Fund (ESF) "Investing in your future," under the 2019 Ramón y Cajal program RYC2019-027683-I and the PID2020-115253GA-I00 HOSTFLOWS project, from Centro Superior de Investigaciones Científicas (CSIC) under the PIE project 20215AT016, and the program Unidad de Excelencia María de Maeztu CEX2020-001058-M. J.D.L. acknowledges support from a UK Research and Innovation Future Leaders Fellowship (MR/T020784/1). This work was funded by ANID, Millennium Science Initiative, ICN12_009. I.D. is supported by the project PID2021-123110NB-I00 financed by MCIN/AEI/10.13039/501100011033/FEDER, UE. Based on observations collected at the Centro Astronómico Hispano en Andalucía (CAHA) at Calar Alto, operated jointly by Junta de Andalucía and Consejo Superior de Investigaciones Científicas (IAA-CSIC). Based on observations made with ESO Telescopes at the Cerro Paranal Observatory under program IDs 095.D-0091(A), 095.D-0091(B), 096.D-0296(A), 097.D-0408(A), 098.D-0115(A), 099.D-0022(A), 0100.D-0341(A), 0101.D-0748(A), 0101.D-0748(B), 0102.D-0095(A), 0103.D-0440(A), 0104.D-0498(A), and 0104.D-0498(B).

This research was supported in part by the University of Pittsburgh Center for Research Computing, RRID:SCR 022735, through the resources provided. Specifically, this work used the H2P cluster, which is supported by NSF award No. OAC-2117681.

Facilities: VLT:Yepun, CAO:3.5m

ORCID iDs

Héctor Martínez-Rodríguez https://orcid.org/0000-0002-1919-228X
Lluís Galbany https://orcid.org/0000-0002-1296-6887
Carles Badenes https://orcid.org/0000-0003-3494-343X
Joseph P. Anderson https://orcid.org/0000-0003-0227-3451
Inmaculada Domínguez https://orcid.org/0000-0002-3827-4731
Hanindyo Kuncarayakti https://orcid.org/0000-0002-1132-1366
Joseph D. Lyman https://orcid.org/0000-0002-3464-0642
Sebastián F. Sánchez https://orcid.org/0000-0001-6444-9307
José M. Vílchez https://orcid.org/0000-0001-7299-8373
Nathan Smith https://orcid.org/0000-0001-5510-2424
Dan Milisavljevic https://orcid.org/0000-0002-0763-3885

References

Abazajian, K. N., Adelman-McCarthy, J. K., Agüeros, M. A., et al. 2009, ApJS, 182, 543
Amorín, R., Vílchez, J. M., Hägele, G. F., et al. 2012, ApJL, 754, L22
Andrews, B. H., Weinberg, D. H., Schönrich, R., & Johnson, J. A. 2017, ApJ, 835, 224
Auchettl, K., Lopez, L. A., Badenes, C., et al. 2019, ApJ, 871, 64
Bacon, R., Vernet, J., Borisova, E., et al. 2014, Msngr, 157, 13
Badenes, C., Harris, J., Zaritsky, D., & Prieto, J. L. 2009, ApJ, 700, 727
Bauer, F. E., Dwarkadas, V. V., Brandt, W. N., et al. 2008, ApJ, 688, 1210
Benetti, S., Pastorello, A., Turatto, M., et al. 2012, ATel, 3969, 1
Bevan, A., Wesson, R., Barlow, M. J., et al. 2019, MNRAS, 485, 5192
Bietenholz, M. F., Bartel, N., Milisavljevic, D., et al. 2010, MNRAS, 409, 1594
Cardelli, J. A., Clayton, G. C., & Mathis, J. S. 1989, ApJ, 345, 245
Castaneda, H. O., Vilchez, J. M., & Copetti, M. V. F. 1990, ApJ, 365, 164
Castrillo, A., Ascasibar, Y., Galbany, L., et al. 2021, MNRAS, 501, 3122
Cid Fernandes, R., Mateus, A., Sodré, L., Stasińska, G., & Gomes, J. M. 2005, MNRAS, 358, 363
Cid Fernandes, R., Pérez, E., García Benito, R., et al. 2013, A&A, 557, A86
Cid Fernandes, R., Schoenell, W., Gomes, J. M., et al. 2009, RMxAA, 35, 127
Dalla Vecchia, C., & Schaye, J. 2012, MNRAS, 426, 140
de Grijs, R., O'Connell, R. W., Becker, G. D., Chevalier, R. A., & Gallagher, J. S. I. 2000, AJ, 119, 681
Dessart, L., Gutiérrez, C. P., Kuncarayakti, H., Fox, O. D., & Filippenko, A. V. 2023, A&A, 675, A33
Diaz, A. I., Terlevich, E., Pagel, B. E. J., Vilchez, J. M., & Edmunds, M. G. 1987, MNRAS, 226, 19
Dwarkadas, V. V. 2005, ApJ, 630, 892
Dwarkadas, V. V. 2007, ApJ, 667, 226
Eibensteiner, C., Barnes, A. T., Bigiel, F., et al. 2022, A&A, 659, A173
Eldridge, J. J., & Xiao, L. 2019, MNRAS, 485, L58
Fox, O., Skrutskie, M. F., Chevalier, R. A., et al. 2009, ApJ, 691, 650
Fox, O. D., Chevalier, R. A., Dwek, E., et al. 2010, ApJ, 725, 1768
Fox, O. D., Fransson, C., Smith, N., et al. 2020, MNRAS, 498, 517
Fransson, C., Chevalier, R. A., Filippenko, A. V., et al. 2002, ApJ, 572, 350
Fransson, C., Lundqvist, P., & Chevalier, R. A. 1996, ApJ, 461, 993
Galbany, L., Anderson, J. P., Rosales-Ortega, F. F., et al. 2016a, MNRAS, 455, 4087
Galbany, L., Anderson, J. P., Sánchez, S. F., et al. 2018, ApJ, 855, 107
Galbany, L., Mora, L., González-Gaitán, S., et al. 2017, MNRAS, 468, 628
Galbany, L., Stanishev, V., Mourão, A. M., et al. 2014, A&A, 572, A38
Galbany, L., Stanishev, V., Mourão, A. M., et al. 2016b, A&A, 591, A48
Hogarth, L., Amorín, R., Vílchez, J. M., et al. 2020, MNRAS, 494, 3541
Holoien, T. W. S., Berger, V. L., Hinkle, J. T., et al. 2023, ApJ, 950, 108
Holoien, T. W. S., Brown, J. S., Vallely, P. J., et al. 2019, MNRAS, 484, 1899
Hopkins, P. F., Kereš, D., Oñorbe, J., et al. 2014, MNRAS, 445, 581
Jennings, Z. G., Williams, B. F., Murphy, J. W., et al. 2014, ApJ, 795, 170
Katsuda, S., Maeda, K., Nozawa, T., Pooley, D., & Immler, S. 2014, ApJ, 780, 184
Kehrig, C., Iglesias-Páramo, J., Vílchez, J. M., et al. 2020, MNRAS, 498, 1638
Kelz, A., Verheijen, M. A. W., Roth, M. M., et al. 2006, PASP, 118, 129
Kiewe, M., Gal-Yam, A., Arcavi, I., et al. 2012, ApJ, 744, 10
Kobayashi, C., Umeda, H., Nomoto, K., Tominaga, N., & Ohkubo, T. 2006, ApJ, 653, 1145
Krühler, T., Kuncarayakti, H., Schady, P., et al. 2017, A&A, 602, A85
Kuncarayakti, H., Anderson, J. P., Galbany, L., et al. 2018, A&A, 613, A35
Kuncarayakti, H., Doi, M., Aldering, G., et al. 2013a, AJ, 146, 30
Kuncarayakti, H., Doi, M., Aldering, G., et al. 2013b, AJ, 146, 31
Kuncarayakti, H., Maeda, K., Anderson, J. P., et al. 2016, MNRAS, 458, 2063
Lacerda, E. A. D., Sánchez, S. F., Cid Fernandes, R., et al. 2020, MNRAS, 492, 3073
Langer, N. 2012, ARA&A, 50, 107
Levenberg, K. 1944, Q. Appl. Math., II, 164, http://www.jstor.org/stable/43633451
Lyman, J. D., Galbany, L., Sánchez, S. F., Anderson, J. P., & Kuncarayakti, H. 2020, MNRAS, 495, 992
Lyman, J. D., Taddia, F., Stritzinger, M. D., et al. 2018, MNRAS, 473, 1359
Mac Low, M. M., & Klessen, R. S. 2004, RvMP, 76, 125
Maoz, D., Mannucci, F., & Nelemans, G. 2014, ARA&A, 52, 107
Markwardt, C. 2012, MPFIT: Robust non-linear least squares curve fitting, Astrophysics Source Code Library, ascl:1208.019
Markwardt, C. B. 2009, in ASP Conf. Ser. 411, Astronomical Data Analysis Software and Systems XVIII, ed. D. A. Bohlender, D. Durand, & P. Dowler (San Francisco, CA: ASP), 251
Marquardt, D. W. 1963, SIAM, 11, 431
Matheson, T., Filippenko, A. V., Ho, L. C., Barth, A. J., & Leonard, D. C. 2000, AJ, 120, 1499
Meza, N., Prieto, J. L., Clocchiatti, A., et al. 2019, A&A, 629, A57
Milisavljevic, D., & Fesen, R. A. 2008, ApJ, 677, 306

Milisavljevic, D., & Fesen, R. A. 2015, Sci, 347, 526
Milisavljevic, D., & Fesen, R. A. 2017, in Handbook of Supernovae, ed. A. W. Alsabti & P. Murdin (Berlin: Springer), 2211
Milisavljevic, D., Fesen, R. A., Chevalier, R. A., et al. 2012, ApJ, 751, 25
Moriya, T. J., Galbany, L., Jiménez-Palau, C., et al. 2023, A&A, 677, A20
Moriya, T. J., Maeda, K., Taddia, F., et al. 2013, MNRAS, 435, 1520
Newville, M., Stensitzki, T., Allen, D. B., et al. 2016, Lmfit: Non-Linear Least-Square Minimization and Curve-Fitting for Python, Astrophysics Source Code Library, ascl:1606.014
Osterbrock, D. E., & Ferland, G. J. 2006, Astrophysics of gaseous nebulae and active galactic nuclei (Sausalito, CA: Univ. Science Books)
Papaderos, P., Gomes, J. M., Vílchez, J. M., et al. 2013, A&A, 555, L1
Patnaude, D. J., Lee, S. H., Slane, P. O., et al. 2015, ApJ, 803, 101
Patnaude, D. J., Lee, S. H., Slane, P. O., et al. 2017, ApJ, 849, 109
Pessi, T., Prieto, J. L., Anderson, J. P., et al. 2023, A&A, 677, A28
Pessi, T., Prieto, J. L., Monard, B., et al. 2022, ApJ, 928, 138
Pettini, M., & Pagel, B. E. J. 2004, MNRAS, 348, L59
Phillips, M. M., Contreras, C., Hsiao, E. Y., et al. 2019, PASP, 131, 014001
Prantzos, N., Abia, C., Limongi, M., Chieffi, A., & Cristallo, S. 2018, MNRAS, 476, 3432
Quirola-Vásquez, J., Bauer, F. E., Dwarkadas, V. V., et al. 2019, MNRAS, 490, 4536
Rigault, M., Copin, Y., Aldering, G., et al. 2013, A&A, 560, A66
Rigault, M., Copin, Y., Aldering, G., et al. 2018, A&A, 612, C1
Rodríguez Del Pino, B., Arribas, S., Piqueras López, J., Crespo Gómez, A., & Vílchez, J. M. 2019, A&A, 630, A124
Romano, D., Karakas, A. I., Tosi, M., & Matteucci, F. 2010, A&A, 522, A32
Roth, M. M., Kelz, A., Fechner, T., et al. 2005, PASP, 117, 620
Sánchez, S. F., García-Benito, R., Zibetti, S., et al. 2016, A&A, 594, A36
Sánchez, S. F., Kennicutt, R. C., Gil de Paz, A., et al. 2012, A&A, 538, A8
Singh, R., van de Ven, G., Jahnke, K., et al. 2013, A&A, 558, A43
Smartt, S. J. 2009, ARA&A, 47, 63
Smith, N. 2014, ARA&A, 52, 487
Smith, N. 2017, in Handbook of Supernovae, ed. A. W. Alsabti & P. Murdin (Berlin: Springer), 403
Smith, N., Kilpatrick, C. D., Mauerhan, J. C., et al. 2017, MNRAS, 466, 3021
Smith, N., Li, W., Filippenko, A. V., & Chornock, R. 2011, MNRAS, 412, 1522
Smith, N., Silverman, J. M., Chornock, R., et al. 2009, ApJ, 695, 1334
Stanishev, V., Rodrigues, M., Mourão, A., & Flores, H. 2012, A&A, 545, A58
Stinson, G., Seth, A., Katz, N., et al. 2006, MNRAS, 373, 1074
Stritzinger, M., Taddia, F., Fransson, C., et al. 2012, ApJ, 756, 173
Strolger, L. G., Rodney, S. A., Pacifici, C., Narayan, G., & Graur, O. 2020, ApJ, 890, 140
Taddia, F., Stritzinger, M. D., Sollerman, J., et al. 2013, A&A, 555, A10
Terlevich, R., Sánchez Portal, M., Díaz, A. I., & Terlevich, E. 1991, MNRAS, 249, 36
Thornton, K., Gaudlitz, M., Janka, H. T., & Steinmetz, M. 1998, ApJ, 500, 95
Thorstensen, J. R., Fesen, R. A., & van den Bergh, S. 2001, AJ, 122, 297
Verheijen, M. A. W., Bershady, M. A., Andersen, D. R., et al. 2004, AN, 325, 151
Vink, J. 2012, A&ARv, 20, 49
Williams, R. M., & Chu, Y. H. 1995, ApJ, 439, 132
Zapartas, E., de Mink, S. E., Izzard, R. G., et al. 2017, A&A, 601, A29